

Can the downward current region of the aurora be simulated in the laboratory?

H Gunell¹, L Andersson², J De Keyser^{1,3}, and I Mann^{4,5}

¹ Belgian Institute for Space Aeronomy, Avenue Circulaire 3, B-1180 Brussels, Belgium

² University of Colorado, Laboratory for Atmospheric and Space Physics, Boulder, Colorado 80309, USA

³ Centre for mathematical Plasma Astrophysics, KU Leuven, Celestijnenlaan 200B, B-3001 Heverlee, Belgium

⁴ EISCAT Scientific Association, P. O. Box 812, SE-981 28 Kiruna, Sweden

⁵ Department of Physics, Umeå University, SE-901 87 Umeå, Sweden

E-mail: herbert.gunell@physics.org

Abstract. A laboratory plasma device is proposed to simulate the downward current region of the aurora. In this device, a discharge in neon is used as a plasma source to represent the hot plasma of the magnetosphere, and a sodium Q-machine source represents the ionospheric plasma. An electrostatic Vlasov model is used to simulate both the downward current region itself and the proposed laboratory analogue. All important phenomena that appear in the simulation of space are found in the laboratory simulation too: a double layer carries most of the potential difference; double layers are in constant motion in the direction of decreasing magnetic field; electron phase space holes appear on the high potential side of double layers and these holes carry a part of the potential difference during double layer disruptions. The ability to simulate auroral physics in the laboratory is better for the downward than the upward current region, because of the lower levels of ion acoustic-like waves in the laboratory model of the former region. Better laboratory–space agreement is found when the discharge and Q-machine ions are of similar masses. If the masses differ significantly, as they do when using helium together with sodium ions, waves on the ion time scale dominate the plasma on the low potential side of the double layer, and there is a tendency toward multiple double layers appearing simultaneously at different locations. The experiment is suitable for the study of heating processes that occur in the downward current region and to address the behaviour of the current–voltage relationship for low voltages.

Keywords Plasma, double layer, aurora, downward current, Vlasov simulation, laboratory experiment, Q-machine

Accepted for publication in *Plasma Phys. Control. Fusion* 24 February 2016.

Published online 8 April 2016, *Plasma Phys. Control. Fusion*, vol. 58, 054003 (2016), doi:10.1088/0741-3335/58/5/054003

1. Introduction

The auroral current circuit comprises the ionosphere, the equatorial magnetosphere, and the upward and downward current regions. The current is driven by a generator, which usually is thought to be located in the magnetosphere [1]. In the upward current region electrons are accelerated downward to cause the well-known light emissions, and in the downward current region electrons are accelerated up into space to close the current circuit.

Double layers have been observed in both the upward [2] and the downward [3] current regions, and they contribute to the electron acceleration. A double layer is a space charge structure, embedded in the plasma, that can carry a large potential drop. The physics of double layers and their formation was reviewed by Raadu [4]. It has been shown that, in a magnetic mirror field configuration, a double layer can have a stable equilibrium position when its polarity is such that it accelerates electrons in the direction towards a stronger magnetic field, and this is the case in the upward current region [5]. This has been confirmed by Vlasov simulations [6]. If there are fluctuations in the circuit, these affect the equilibrium and may cause fluctuations in both the double layer voltage and position [7]. In the downward current region no stable equilibrium exists, and therefore the double layers are always in motion even for stationary boundary conditions [8]. Observations by the Fast Auroral Snapshot (FAST) spacecraft in the downward current region were explained using a pressure-cooker model. In a pressure-cooker model an electric field confines ions to low altitudes, where they are heated by waves until their energy is large enough to allow them to escape [9]. A modified pressure-cooker model was later proposed, replacing the static electric field by moving double layers [10].

Laboratory experiments on electric fields parallel to the magnetic field in magnetic mirror configurations have been performed in Q-machines [11, 12] and particle in cell simulations have been used to model the experiments [13]. Double layers have also been seen in laboratory experiments [14, 15, 16, 17]. Waves on the electron time scale that appear on the high potential side of double layers have been studied using theory, simulations, and laboratory experiments [18, 19, 20, 21].

Gunell, et al. [22] proposed an experiment to simulate the upward current region in the laboratory. Using Vlasov simulations of both the space and laboratory environments it was shown that similar potential profiles, involving double layers, form in both the laboratory and space systems. It was also found that ion acoustic waves that are heavily damped in space are only weakly damped in the laboratory, and

that the acceleration voltage should be chosen so that the excitation of ion acoustic waves is kept low.

In this paper, we conduct electrostatic Vlasov simulations in order to investigate whether this kind of device can be used to study the physics of not only the upward, but also the downward current region of the aurora. By using Vlasov simulations we include kinetic phenomena such as phase space holes that have been shown to be part of the double layer disruptions that occur in the downward current region [8, 23].

2. Simulation model

We use an electrostatic Vlasov simulation code [6], which is one-dimensional in configuration space and two-dimensional in velocity space. The spatial dimension is the coordinate z along the magnetic field line, where $z = 0$ is at the magnetic equator and $z = 5.5 \times 10^7$ m is at 120 km altitude in the ionosphere. In the simulations of the laboratory device, $z = 0$ and $z = 3$ m are at the corresponding ends of the main plasma chamber as shown in figure 1. The velocity dimensions are represented by the velocity v_z parallel to the magnetic field and the magnetic moment $\mu = mv_{\perp}^2 / (2B(z))$. Thus, we write the distribution function $f(z, v_z, \mu, t)$, and because the magnetic moment is an adiabatic invariant we have $\dot{\mu} = 0$. The $\dot{\mu} = 0$ approximation is valid as long as the change of B experienced by a particle is insignificant over one gyrotational period. This has been verified for the space case by performing three-dimensional test particle simulations where the $\dot{\mu} = 0$ approximation was not used [6]. For the simulations of the experimental device presented here the parallel velocity is low enough for $\dot{\mu} = 0$ to hold for all electrons and all thermal ions. There is a minority of accelerated ions that may reach parallel speeds that could yield a significant magnetic field change in over gyration. However, these ions stay at high $|v_z|$ values only for short periods of time, and test particle simulations show that the total change in μ over $200 \mu\text{s}$, which is longer than the duration of the Vlasov simulations, is less than 4.7%. Therefore a constant μ is a reasonable approximation also for the ions. Implications for the magnetic design of an experimental device are discussed in Appendix B.

The forces that are included in this model come from the magnetic mirror field, the parallel electric field, and, in the space case, the gravitational field. When simulating the laboratory experiment the gravitational acceleration a_g is set to zero. We solve a system constituted by the Vlasov equation and a Poisson type equation adapted to the magnetic field

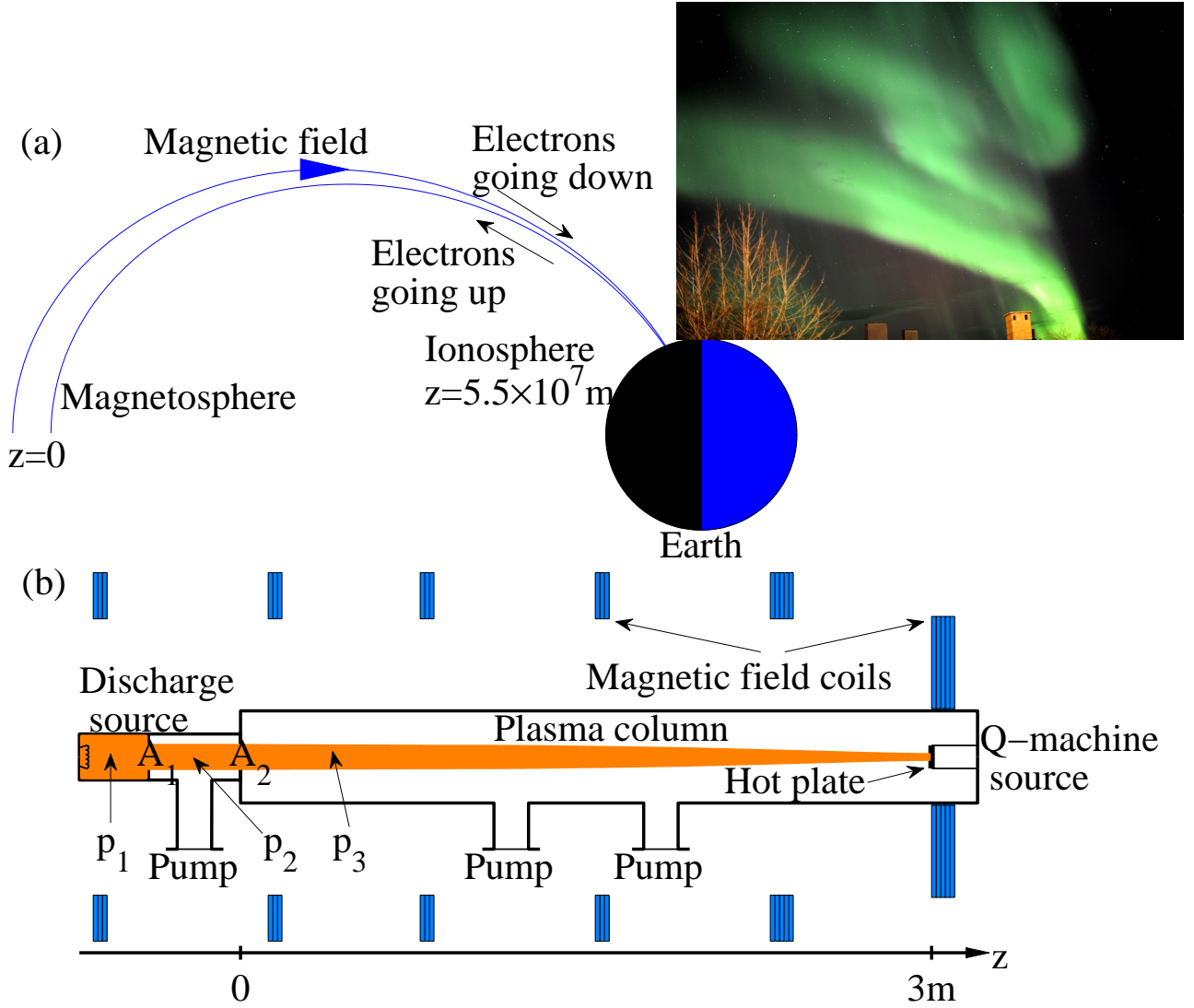


Figure 1. Schematics of the two simulated systems. (a) An auroral field line. The equatorial magnetosphere is at $z = 0$ and the ionosphere at $z = 5.5 \times 10^7$ m, which corresponds to an altitude of 120 km. The photograph shows an aurora in Kiruna in Sweden 2 October 2013. (b) Laboratory experiment. On the left a gas discharge represents the plasma of the magnetosphere, and on the right a Q-machine source represents the ionosphere. The pressures in the different sections of the vacuum vessel, p_1 , p_2 , and p_3 , and the cross sections of the apertures, A_1 and A_2 , are used in the pressure estimate in Appendix A.

geometry:

$$\frac{\partial f}{\partial t} + v_z \frac{\partial f}{\partial z} + \frac{1}{m} \left(qE - \mu \frac{dB}{dz} + ma_g \right) \frac{\partial f}{\partial v_z} = 0, \quad (1)$$

$$\frac{d}{dz} \left(\frac{B_S}{B} E \right) = \frac{\rho_l}{S \epsilon_r \epsilon_0}, \quad (2)$$

where S is the flux tube cross section at a reference point, and B_S is the magnetic flux density at that point. In (2), ρ_l is the charge per unit length of the flux tube. It is found by integrating the distribution functions over velocity space for all species s :

$$\rho_l = \sum_s q_s \int f_s(v_z, \mu) d\mu dv_z. \quad (3)$$

On the right-hand side of (2) an artificial relative

dielectric constant ϵ_r has been introduced in order to reduce the computational effort. It allows larger grid cells and longer time steps, because $\lambda_D \sim \sqrt{\epsilon_r}$ and $\omega_p \sim 1/\sqrt{\epsilon_r}$. A consequence of having $\epsilon_r > 1$ is that the widths of double layers and phase space holes are overestimated by a factor of $\sqrt{\epsilon_r}$. However, if these widths are kept small in comparison with typical length scales for the overall changes of the plasma properties, the exact values of the widths are not important for the results of the simulation. In the simulations of space, reported in section 3, $\epsilon_r = 8100$ is used. In the simulations of the laboratory experiment, reported in section 4, the overall demand on computational resources is less severe, allowing the natural $\epsilon_r = 1$

Table 1. Parameters used in the simulations at the magnetospheric and ionospheric boundaries in space and the discharge and hot plate ends of the laboratory device.

	Space		Laboratory	
	Magnetosph.	Ionosphere	Discharge	Hot plate
z	0	5.5×10^7 m	0	3 m
B	$0.086 \mu\text{T}$	$56 \mu\text{T}$	0.02 T	0.5 T
V	0	-400 V	0	-(10-25) V
$k_{\text{B}}T_{\text{e}}$	125 eV	50 eV	10 eV	(1-2) eV
$k_{\text{B}}T_{\text{i}}$	625 eV	50 eV	0.03 eV	(1-2) eV
ion	H^+	H^+	He^+, Ne^+	Na^+
n_{e}	$3 \times 10^5 \text{ m}^{-3}$	10^9 m^{-3}	10^{14} m^{-3}	10^{15} m^{-3}

to be used. For example, the width of the double layer in the space simulation, shown in figure 2(*d*) below, is 150 km, and the effective Debye length at the double layer position is 3.4 km. As $\epsilon_{\text{r}} = 8100$ the scaling factor is 90, and the predicted double layer width and Debye length in space would be 1.7 km and 38 m respectively. In the simulation of the laboratory experiment, in figure 4(*a*), the double layer width is 23 mm and the Debye length 0.3 mm. In both cases the value of the Debye length is taken from the low potential side, where it is shorter than on the high potential side. These values are in agreement with the double layer widths of ‘‘some tens of plasma Debye lengths’’ that were reported from laboratory experiments [15].

A stationary magnetic field is prescribed. For the space simulations we use an approximation of the $L = 7$ shell of a magnetic dipole field. This corresponds to the geometry that is illustrated in figure 1(*a*). For the laboratory simulations we use a field that can be generated by the coils in figure 1(*b*). The model being electrostatic, Alfvén waves are not included in our results, and we are restricted to the study of electrostatic aspects of the aurora. More information about the simulation model can be found in [6].

3. The downward current region

In our previous paper on the downward current region, five different simulation runs for the downward current region were presented [8]. Here we present one case, for which we outline the physics, and then we compare these results to simulations of the laboratory setup in section 4. The parameters at the boundaries of both the space and laboratory cases are shown in table 1. In the simulations of the space plasma all ions that we simulate are protons, and the simulation also includes electrons. Populations entering the simulated region from the two boundaries are treated as different species. Thus we have four species: electrons from the magnetosphere; ions from the magnetosphere; electrons from the ionosphere, and

ions from the ionosphere. At $t = 0$ the system was filled with a constant density ($n = 3 \times 10^5 \text{ m}^{-3}$) of the magnetospheric species. The initial density of the ionospheric species was zero throughout the system. For $t > 0$ both ions and electrons from the ionosphere are allowed to enter the system. The initial distribution functions are Maxwellian, and the distributions at the boundaries are Maxwellian throughout the simulation. The total potential difference indicated in table 1 is kept constant during the course of the simulation.

In the downward current region there are heating processes at work which cannot be modelled self-consistently within an electrostatic model. Instead we set the temperature of the ionosphere to 50 eV as a boundary condition. This produces plasma temperatures that are consistent with the observations by Andersson et al. [3] at the altitude where these observations were made. The main difference between the simulations reported in this section and those previously published [8] is that the temperature of the species that have their origin at the magnetosphere is lower here by a factor of 4. The observations of double layers in the downward current region do not put severe constraints on the temperature of these species [3], and we lowered the temperature, within the limits of what is realistic, to see how that influences the results.

Figure 2 shows a summary of a computer simulation of the downward current region. At $t = 75$ s it is seen in figure 2(*d*), which shows the plasma potential as a function of z , that a double layer is present at $z = 5.0 \times 10^7$ m (altitude approximately 5100 km) where there is sharp potential drop. Double layers are created by instabilities when the relative drift velocity between the ion and electron populations becomes too large. In this way a field aligned potential drop can be supported in a collisionless plasma. It is seen in figure 2(*g*) that electrons from the ionosphere are accelerated by the double layer voltage, forming a beam on the high potential side. The beam travels through a narrow gap region, without significant electric fields. Such a gap region has been observed by satellites [3] and in laboratory experiments [14, 18]. When a distinct gap region exists, there is a laminar flow of electrons through the double layer. We call this a laminar double layer. When a double layer is disrupted, the electron flow becomes turbulent, and that is called a turbulent double layer [24].

Beyond the gap, electron phase space holes are formed by the interaction between the electron beam and the electrons of the background plasma. These holes are seen in both the ionospheric and magnetospheric electron populations in figures 2(*g*) and 2(*e*) respectively. The net charge of the electron holes is positive, and the corresponding positive peaks in the plasma potentials are seen in figure 2(*d*).

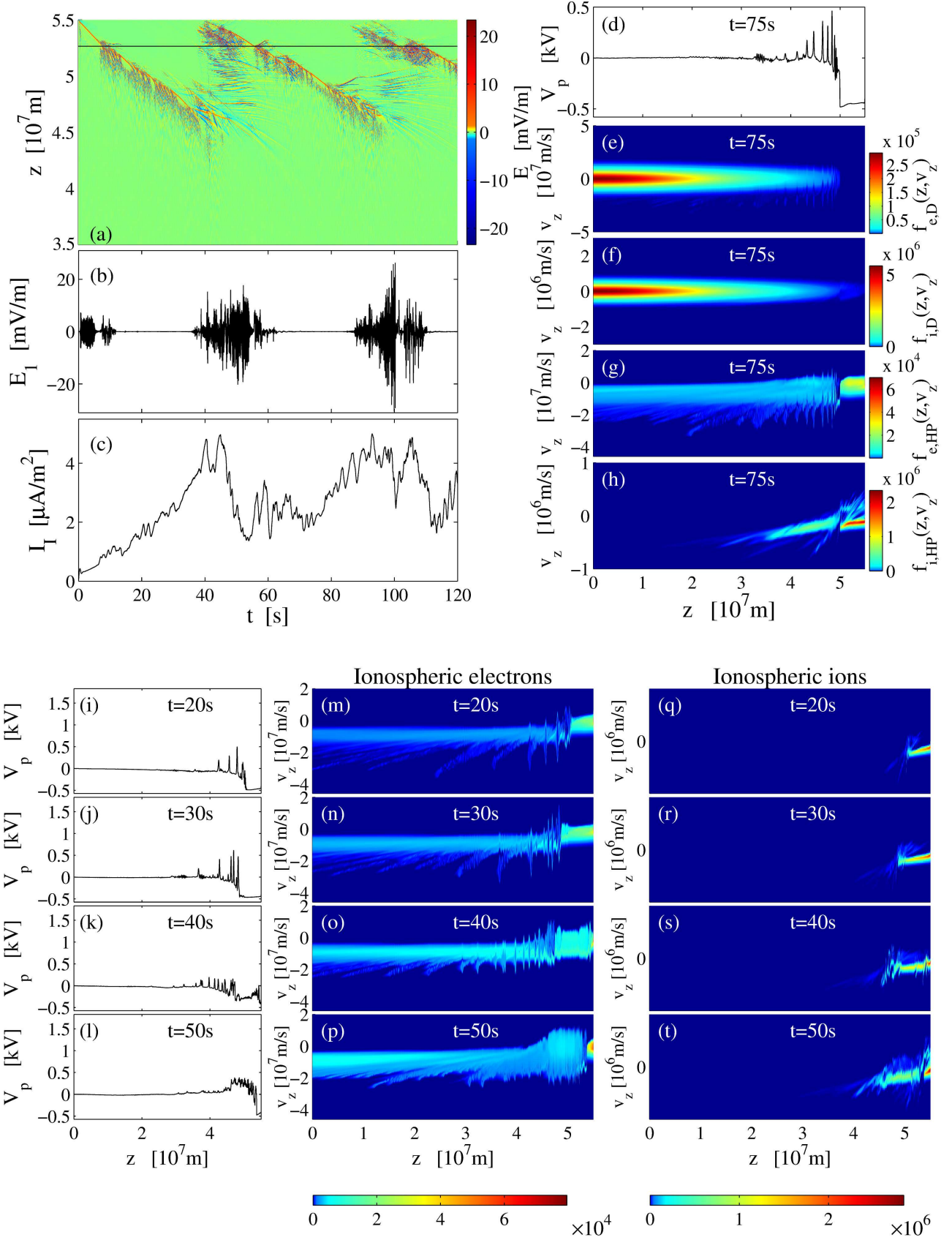


Figure 2. Summary of the Vlasov simulation of the downward current region of the aurora. (a) The electric field in a $z-t$ diagram for $z \geq 3.5 \times 10^7$ m. (b) Electric field at $z = 5.265 \times 10^7$ m (altitude 2470 km). This position is indicated by the horizontal black line in panel (a). (c) Current density scaled to the ionospheric side of the system. (d) Plasma potential as a function of z at $t = 75$ s. (e-h) phase space densities for (e) magnetospheric electrons; (f) magnetospheric protons; (g) ionospheric electrons; and (h) ionospheric protons. (i-l) Plasma potential for $t = 30, 40, 50$, and 60 s. (m-p) Phase space density for ionospheric electrons for $t = 30, 40, 50$, and 60 s. (q-t) Phase space density for ionospheric protons for $t = 30, 40, 50$, and 60 s. All phase space densities, $f(z, v_z)$, have been normalised so that integrals over all v_z yield n_s/B . The unit for $f(z, v_z)$, shown by the colour scales in panels (d-g) and (l-s) is $\text{m}^{-4}\text{T}^{-1}\text{s}$.

Ions on the high potential side are accelerated in the double layer toward lower altitudes. This is seen in figure 2(*h*), where the accelerated ions form a beam on the low potential side. The beam interacts with the ion background, and this leads to the breakup of the beam and to heating of the ionospheric ion population. While the breakup of the beam itself can be interpreted as heating of the ions, more effective perpendicular heating processes are not included in the present model. Instead the temperature at the ionospheric boundary is kept at $k_B T = 50$ eV, which gives temperatures in agreement with observations at the altitudes where these took place. Ion acceleration is seen also in figure 2(*f*), but since the magnetospheric ions are warmer no distinct beam is formed.

The generalised Langmuir condition is an existence criterion, which requires a balance of the total pressure across the double layer [4]. If this can be satisfied only in a moving frame of reference, the double layer is forced to move. It has been shown that in a magnetic mirror configuration, a stable equilibrium double layer position can exist if the electrons are accelerated toward the stronger magnetic field, as in the upward current region, and that this equilibrium is unstable if the electrons are accelerated toward the weaker magnetic field, as in the downward current region [5]. The stability argument is based on the different behaviours of the species that enter the magnetic mirror from its two ends. The density of the magnetospheric species is approximately constant, while the density of the ionospheric species decreases as the flux tube expands when they move into regions of weaker magnetic field. Double layer motion is also discussed in [8].

The motion of the double layer can be followed in figure 2(*i-l*), showing the plasma potential as a function of z for times $t = 20, 30, 40,$ and 50 s; panels (*m-p*) show the corresponding phase space densities $f(z, v_z)$ of the ionospheric electrons; and panels (*q-t*) show phase space densities of ionospheric ions. The double layer moves upward (toward lower z values) until it is disrupted, then a new double layer is formed near the ionosphere, and the process repeats itself. It is seen in figure 2(*k*) that at $t = 40$ s a new double layer has just formed at $z \approx 5.45 \times 10^7$ m (altitude 635 km), close to the right-hand end of the figure. At the same time the old double layer is about to fade away at $z \approx 4.74 \times 10^7$ m (altitude 7.7×10^3 km). The reason for this disruption of the double layer is that as it reaches a high enough altitude, the density of the ionospheric electrons has fallen so much, by expansion of the flux tube in the decreasing magnetic field, that the Langmuir condition can no longer be satisfied [8]. During the disruption a larger part of the voltage drop is carried by the phase space holes than

by the double layer. The ambipolar electric field on the low potential side, seen as a positive slope on the plasma potential curve in figure 2(*i*), vanishes during the disruption. When it does, the electron–ion relative velocity increases at low altitude, creating favourable conditions for double layer formation in that region.

The double layer motion is also seen in the $z-t$ diagram of the electric field in figure 2(*a*), where the large spotted regions are dominated by electron phase space holes, and the double layer is represented by the high z edge of that region. The electric field associated with the electron holes cannot be resolved completely on the scale of the figure, and this is the reason for its spotty appearance. The electron beam–plasma interaction that gives rise to the electron holes affect the magnetospheric electrons more than in the previous paper [8]. We see holes in the magnetospheric electron population, shown in figure 2(*e*). In the previous paper, holes mostly appeared in the ionospheric electron population. The difference is that the temperature of the magnetospheric species is lower in the present simulation. The phase space density of the bulk magnetospheric electron population at the velocity at which the holes move, about -2×10^7 ms⁻¹, is therefore lower here than in [8]. This enables holes to form more easily in the minority magnetospheric electron population that has been accelerated to the same velocity range as the ionospheric electrons, there being fewer thermal electrons resonant with the wave electric field that moves with the velocity of the holes. The electric field associated with the electron holes is seen in figure 2(*b*), which shows the electric field E_1 as seen by a stationary observer at $z = z_1 = 5.265 \times 10^7$ m (altitude 2470 km). This position is indicated by the horizontal black line in panel (*a*). The altitude 2470 km was chosen because it is where double layers were observed in the downward current region by the FAST satellite [3]. Both the amplitude of the wave field and its temporal dependence is similar to that of the simulations in [8].

The current density, shown in figure 2(*c*), oscillates around a mean value. Because it is the electrons from the ionosphere that carry most of the current, this mean value is determined by the density and temperature at the ionospheric boundary. The fundamental period of the oscillations is the same as the recurrence period of the double layer reformation process. The current increases as the double layer moves away from the ionosphere, and it reaches its maximum at the time of the double layer disruptions, which also is when the ambipolar electric field on the low potential side vanishes. The ambipolar field acts to decrease the speed of the upflowing ionospheric electrons. When the ambipolar electric field vanishes, the electrons can move faster and carry a larger

current. The increased electron speed also means that the relative velocity between the electrons and ions increases, and that favours double layer formation at low altitudes. There is no simple current–voltage relationship in the downward current region, and rather than the voltage it is the ionospheric conditions that set the limit to the current. However, these ionospheric conditions may depend on both the voltage and current in the auroral current circuit.

4. Laboratory experiments

4.1. General description

An experimental setup intended to simulate the upward current region in the laboratory was proposed not long ago [22]. Here we use computer simulations to explore the possibility of using the same configuration to study the downward current region. A schematic of the device is shown in figure 1(b), and basic parameters are shown in table 1. In this laboratory experiment, the magnetospheric source is represented by a discharge on the left-hand side of the machine. The discharge provides a plasma with an electron temperature $k_B T_e = 10$ eV. The plasma corresponding to the ionosphere is created by a Q-machine source on the right-hand side. A review of Q-machines and their contribution to the auroral physics has been published by Koepke [25]. In a Q-machine plasma emerging from the hot plate, both the electron and ion temperatures are equal to the temperature of that hot plate – about 2000 K. However, temperatures corresponding to several electron volts have been measured in Q-machines as a result of current-driven instabilities [26]. Since perpendicular heating cannot be included self-consistently in our model, we instead increase the temperature of the hot plate plasma to 1–2 eV as a boundary condition. It was seen in simulations of the downward current region in space that increasing the temperature at the ionospheric boundary yields realistic temperatures within the range that has been observed by satellites [8].

Phase space holes are predicted in section 4.2 below for both ions and electrons. The decay of such holes due to collisions with the neutral gas was studied experimentally for electrons [27] and in simulations for ions [28]. Estimating the pressure that can be obtained in the main chamber of the device in figure 1, we find that it can be kept low enough to avoid collisional damping of phase space holes if the diameter of the apertures is 10 cm and that of the pumps 15 cm. The details of the calculation and the comparison with [27] and [28] are found in Appendix A.

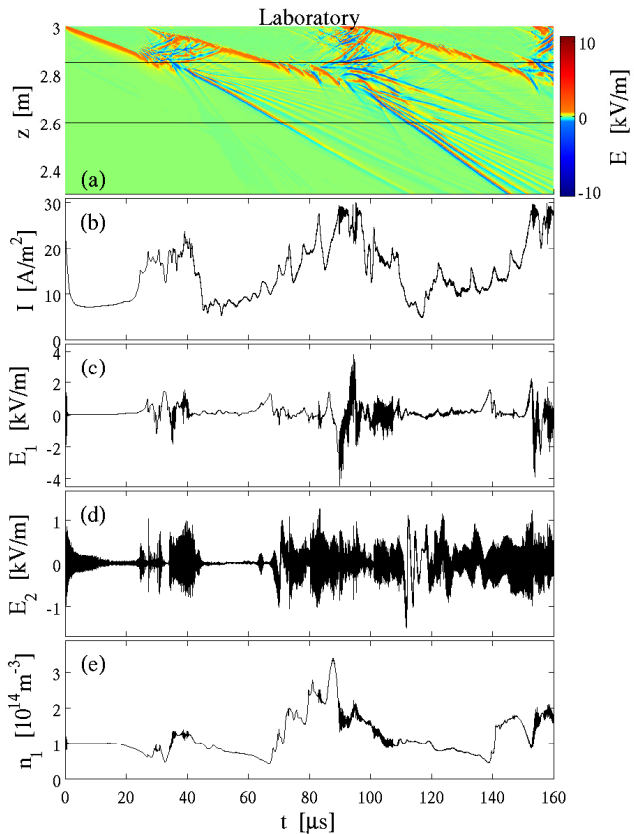


Figure 3. A computer simulation of a laboratory experiment with Ne^+ and Na^+ ions. The voltage across the system is 25 V, the density at the hot plate $4 \times 10^{15} \text{ m}^{-3}$, and the temperature at the hot plate $k_B T = 1$ eV. (a) The electric field in a $z - t$ diagram for $z \geq 2.3$ m. (b) Current density scaled to the position of the hot plate ($z = 3$ m). (c) Electric field E_1 at $z_1 = 2.85$ m. (d) Electric field E_2 at $z_2 = 2.7$ m. (e) Plasma density n_1 at $z_1 = 2.85$ m. The coordinates z_1 and z_2 are indicated by the black lines in panel (a).

4.2. Simulation results

Results from a simulation of the proposed experiment are shown in figures 3, 4, and 5. The density at the hot plate side ($z = 3$ m) is $1 \times 10^{15} \text{ m}^{-3}$ and the temperature $k_B T = 1$ eV. The discharge source is kept at a potential of 0 V and the hot plate at -25 V. It is seen in the $z - t$ diagram of the electric field in figure 3(a) that a double layer forms at the hot plate and moves toward lower z , where the magnetic field is weaker. The double layer is then disrupted, and subsequently a new one forms near the hot plate. This behaviour is analogous to that of the downward current region shown in figure 2. The same is true of the current density shown in figure 3(b). The current density oscillates around a mean value, and the principal period of the oscillations is that of the recurrence period of the double layer formations. Also the electric field and plasma density at $z = z_1 = 2.85$ m shown in figures 3(c) and 3(e) have the same properties

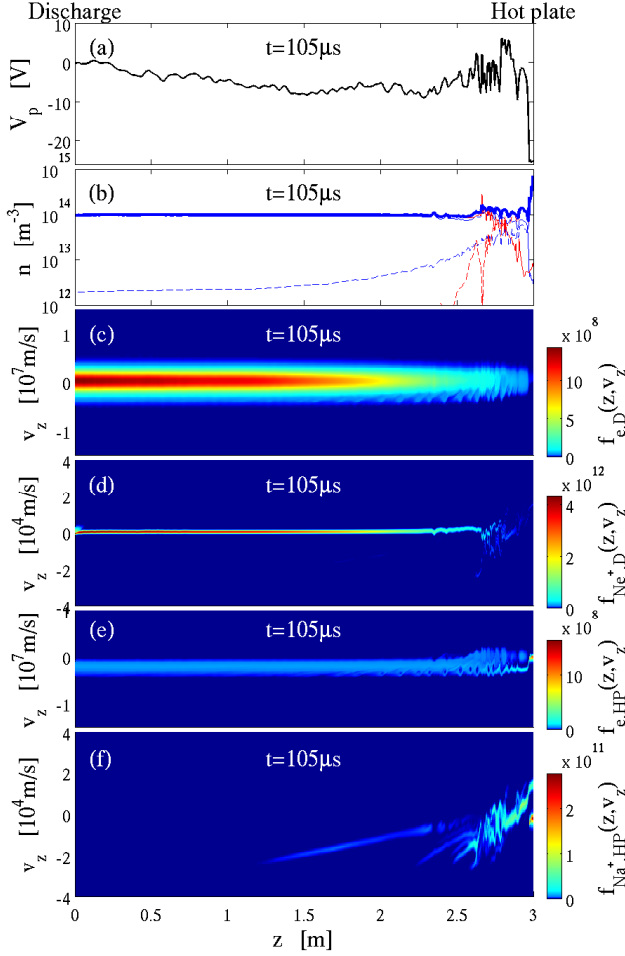


Figure 4. The state at $t = 105 \mu\text{s}$ of the simulation run shown in figure 3. (a) Plasma potential as a function of z . (b) Densities as functions of z . The thick blue curve shows the plasma density. The thin solid curves show Ne^+ ions (red) and electrons (blue) from the discharge end of the system. The dashed curves show Na^+ ions (red) and electrons (blue) originating from the hot plate. (c)–(f) Phase space densities for (c) electrons from the discharge; (d) Ne^+ ions from the discharge; (e) electrons from the hot plate; and (f) Na^+ ions from the hot plate. The colour scales have been normalised so that integrals over all v_z yield n_s/B . The unit for $f(z, v_z)$ is $\text{m}^{-4} \text{T}^{-1} \text{s}$. A video clip showing the information in this figure for $t \leq 160 \mu\text{s}$ is available online.

as the corresponding quantities in the simulations of auroral field lines. The double layer passage can be seen as a positive electric field at $z = z_1$ in figure 3(c), and, particularly around times of double layer disruption, there are electric field oscillations at high frequencies. The density at $z = z_1$ increases after a double layer passage, as z_1 then is located in the dense plasma emerging from the hot plate.

Figure 4 shows the situation at $t = 105 \mu\text{s}$ in the same simulation run as that in figure 3. In figure 4(a) the double layer is seen as the potential drop close to the hot plate, where it had been formed just before, and, as one can see in figure 4(a), it is moving in

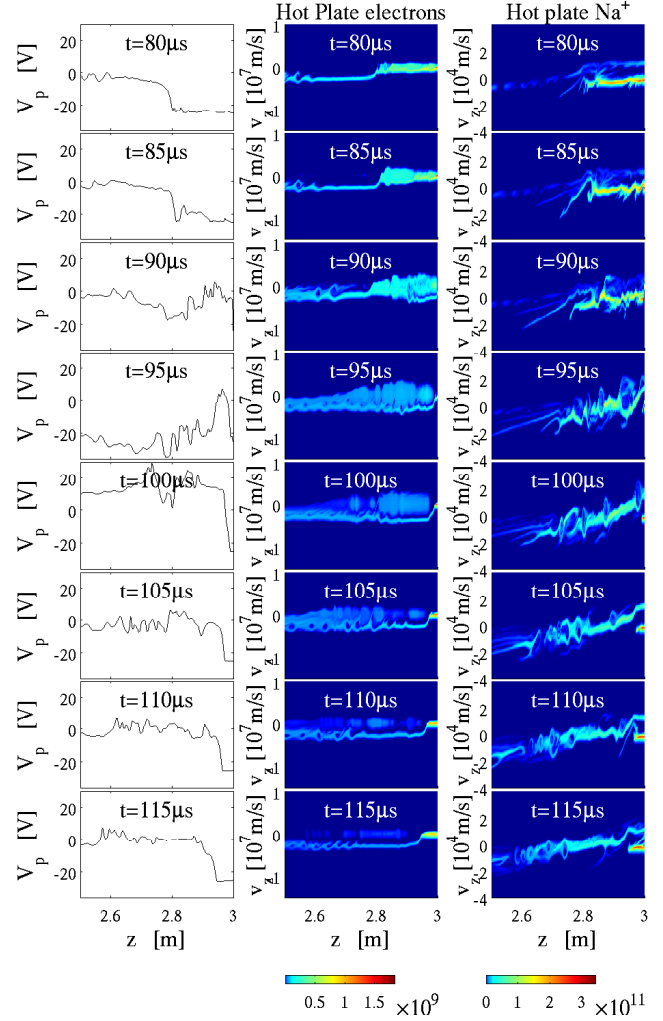


Figure 5. Reformation of a double layer in the same simulation run as in figures 3 and 4. The left column shows the plasma potential, the middle column the phase space density of the electrons from the hot plate, and the right column the phase space density of Na^+ ions from the hot plate for a succession of times from $t = 80 \mu\text{s}$ to $t = 115 \mu\text{s}$ as indicated on each panel. Only the range $2.5 \text{ m} < z < 3 \text{ m}$ is shown. The colour scales have been normalised so that integrals over all v_z yield n_s/B . The unit for $f(z, v_z)$ is $\text{m}^{-4} \text{T}^{-1} \text{s}$.

the direction of lower z values. The waves that are generated by electron beam–plasma interaction on the high potential side are seen in the potential curve and in both the plasma density in figure 4(b) and the electron phase space plots in panels (c) and (e). Phase space holes are seen in both electron populations. In figure 4(f) Na^+ ions are seen to be accelerated in the double layer back toward the hot plate. Phase space structures are also seen at $z \approx 2.7 \text{ m}$ in panel (d) for the Ne^+ ions from the discharge, and a hole is seen at that location in the Na^+ population in panel (f). The hole formed in the turbulence of the double layer disruption during the interval $90 \mu\text{s} \lesssim t \lesssim 100 \mu\text{s}$.

In order to illustrate the reformation figure 5 shows a sequence of plasma potential and phase space densities for the species coming from the hot plate from $t = 80 \mu\text{s}$ to $t = 115 \mu\text{s}$. One difference between the behaviour of the laboratory and space plasmas is that there are more ion phase space holes formed in the laboratory than in the space environment. The laboratory ion populations in the right column of figure 5 are more affected by wave-particle interaction than are the ion populations in space shown in figure 2($q-t$). Ion acoustic waves are heavily damped on auroral field lines, since there the ion temperature is greater than or equal to the electron temperature. In the proposed laboratory experiment, ions and electrons coming from the Q-machine source have equal temperature, while the Ne^+ ions from the discharge source are much colder than the electrons due to charge-exchange collisions with the neutral gas in the source itself. This enables wave activity on ion timescales in the region where Ne^+ is the dominating ion species on the high potential side of the double layer. Perturbations of the Ne^+ ion populations are seen in figure 4(d). Once waves on the ion time scale are launched, these affect also the Na^+ ions, which is seen in figure 4(f). The large ion perturbations in the right column of figure 5 all appear on the high potential side of the double layer. On the low potential side, between the double layer and the hot plate, Na^+ ions dominate, the electron and ion temperatures are equal, and there the ion beam-plasma interaction is similar to the space case.

After the reformation of the laminar double layer, for $100 \mu\text{s} \leq t \leq 115 \mu\text{s}$, there is a potential minimum at the foot of the double layer and an ambipolar electric field is present on the low potential side. In the lowermost left panel of figure 5 there is approximately 0.6 V over 4 cm of the low potential side. This ambipolar potential drop is on the order of the voltage equivalent of the temperature at the hot plate boundary, which in this simulation was $k_{\text{B}}T/e = 1 \text{ V}$. A similar ambipolar potential drop is seen in the space simulation in figure 2(d), where approximately 40 V could be associated with the ambipolar field and the temperature at the ionospheric boundary was 50 eV.

The amplitude of the high-frequency electric field oscillations at $z = z_1 = 2.85 \text{ m}$ during the double layer disruption is approximately of the same magnitude as the electric field in the double layer. The amplitude of the electron time scale waves on the high potential side of the double layer when it is in a laminar state, for example when it passes z_1 at $t = 139 \mu\text{s}$, is much lower. This is seen in figure 3(c) for $120 \mu\text{s} \lesssim t \lesssim 135 \mu\text{s}$ when z_1 was on the high potential side. In the same interval the amplitude at $z = z_2 = 2.6 \text{ m}$ reaches about 1 kV/m as seen in figure 3(d). In figure 3(a) the high-

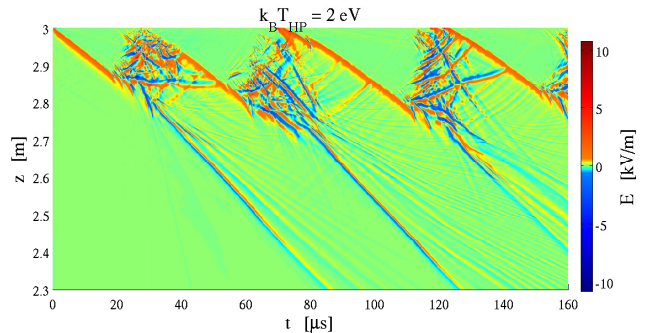


Figure 6. Raised temperature at the right-hand boundary. The figure shows the electric field in a $z-t$ diagram for $z \geq 2.3 \text{ m}$ in a simulation of a plasma, where the temperature of the electrons and Na^+ ions from the hot plate is $k_{\text{B}}T = 2 \text{ eV}$. The other parameters are the same as in the run shown in figures 3–5.

frequency oscillations have been suppressed by the low-pass filtering that has been applied in postprocessing to accommodate the full $160 \mu\text{s}$. In space the gap region is much smaller than the distance over which the double layer moves. Therefore both the high-frequency waves and the double layer can be observed consecutively at the same position. In the laboratory the sizes of the gap and the region where double layers are found are of the same order of magnitude, and observations of electron timescale waves and laminar double layers should be made at different positions.

In order to examine the effects of heating of the low potential plasma, a simulation was run with an increased temperature of the plasma emerging from the hot plate. While the other parameters were kept unchanged from the run presented in figures 3–5, the temperature at the right-hand boundary was set to $k_{\text{B}}T = 2 \text{ eV}$ for both electrons and ions. A $z-t$ diagram of the electric field in this run is shown in figure 6 for $z \geq 2.3 \text{ m}$. The only significant difference between figure 6 and figure 3(a) is that the double layer moves at a higher speed in figure 6, where the temperature is higher. The hotter plasma expands faster, and this allows the double layer to move faster. What the exact velocity becomes is determined by the interaction between the double layer and the expanding plasma on its low potential side [8].

The results presented so far in this paper, and all results in [22], have been for a sodium Q-machine source and a discharge in neon. These species were chosen because the sodium and neon ions have similar masses, $m_{\text{Ne}} = 20 \text{ u}$ and $m_{\text{Na}} = 23 \text{ u}$. In space, above altitudes of a few hundred kilometres, the dominating ion species is H^+ . While it therefore is reasonable to choose ions with similar masses, it is also interesting to see what the consequences of a different choice would be. Figure 7 shows an example of the results of a simulation of an experiment where the magnetospheric

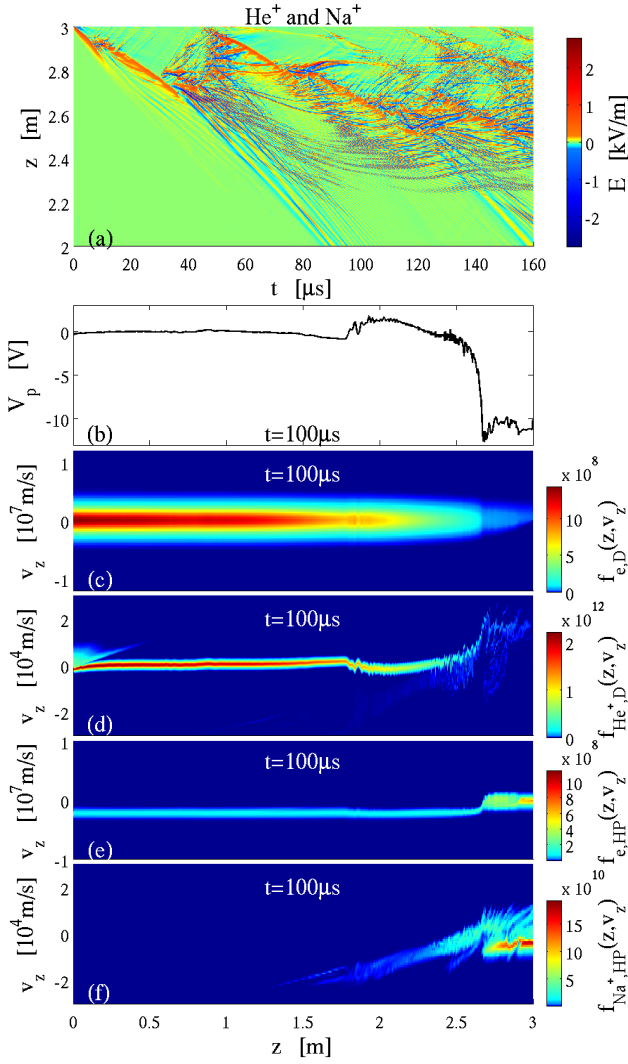


Figure 7. In this simulation, the discharge ions are He⁺; the potential of the hot plate is -10 V; and the temperature of the electrons and Na⁺ ions from the hot plate is $k_B T = 2$ eV. (a) The electric field in a $z - t$ diagram for $z \geq 2$ m. (b)–(e) Phase space densities at $t = 100 \mu\text{s}$ for (b) electrons from the discharge; (c) He⁺ ions from the discharge; (d) electrons from the hot plate; and (e) Na⁺ ions from the hot plate. The colour scales have been normalised so that integrals over all v_z yield n_s/B . The unit for $f(z, v_z)$ is $\text{m}^{-4} \text{T}^{-1} \text{s}$.

source was represented by a discharge in helium. The ion were thus He⁺ and Na⁺. After the first double layer disruption at $t = 40 \mu\text{s}$ in figure 7(a) ion timescale waves with wavelengths on the order of centimetres appear near the place where the double layer was disrupted. They propagate slowly, but at the end of the run at $t = 160 \mu\text{s}$ they fill the whole region that repeatedly is traversed by double layers. There is an increasing tendency toward multiple double layers appearing simultaneously at different locations. The waves are also seen in the ion phase space density diagrams in figures 7(d) and (f). We conclude that

these waves are a result of the difference in ion mass, since they are absent in the simulation runs where the ion masses are similar.

The presence of these waves also affect the potential curve shown in figure 7(b). In the simulation of space and in that of the experiment with similar ion masses the potential curves are smooth on the low potential side and dominated by the ambipolar electric field, except during disruptions. In the He⁺–Na⁺ setup, on the other hand, waves are seen at an amplitude on the same order of magnitude as the ambipolar potential drop. Nevertheless there is a potential minimum at the foot of the double layer, and thus the average field is similar to the ambipolar field seen in the simulation of the experiment with Ne⁺ and Na⁺ ions. Figure 7(b) shows the potential for $t = 100 \mu\text{s}$, and – as figure 7(a) shows – the low potential plasma becomes more dominated by waves for $t > 100 \mu\text{s}$. Thus the average field may be difficult to observe experimentally in the plasma with dissimilar ion masses.

5. Conclusions

We have conducted simulations of both the downward current region of the aurora and a proposed laboratory experiment intended to model that part of space. In both environments the voltage is carried by a double layer that moves in the direction where the magnetic field is weaker. The double layer is disrupted when it reaches a point where the density of the electrons entering from the low potential side becomes so low that the Langmuir condition no longer can be satisfied. Then a new double layer forms near the ionosphere or, in the laboratory case, the hot plate. In both systems, the current exhibits oscillations around a mean value, and the fundamental period is the same as that of the double layer reformation. In conclusion, the large spatial scale, long timescale, behaviour is the same in the laboratory as in space, and the proposed experiment is a good model of the downward current region. In fact, the agreement between the two systems found here is better than that found in simulations of the upward current region [22].

In the upward current region, ions coming from the ionosphere are accelerated in a double layer and travel upward as ion beams. When interacting with the background plasma, these beams give rise to ion time scale waves. The damping of these waves is strong in the magnetosphere, because of the large ion to electron temperature ratio. In the laboratory, the ions formed in the discharge are much colder than the electrons, which leads to the creation of large amplitude waves through ion beam–plasma instabilities. However, it was found that these instabilities could be avoided by

adjusting the acceleration voltage so that the ion beam speed is sufficiently different from the ion acoustic speed [22]. In the downward current region, the ion beams travel through the plasma that emerges from the ionosphere, in space, or the hot plate in the laboratory analogue. In both these plasmas the ion to electron temperature ratio is close to unity, and that is the reason for the better agreement in modelling the downward current region.

In both the laboratory and in space, ions follow the double layer on its low potential side moving in the negative z direction. When the double layer is disrupted and forms anew at high z these ions are left on the high potential side of the newly formed double layer. Some of them are accelerated toward higher z in the new double layer and contribute to the heating of the low potential plasma through ion beam–plasma interaction. Those that remain on the high potential side continue to move upward. In the space case, some phase space perturbations can be seen in figures 2(*s*) and 2(*t*). These ions are located in the region where the dominating plasma populations have their respective sources at $z = 0$. In the laboratory, this means that the electron temperature is much larger than the ion temperature, and therefore the ion timescale perturbations are larger, and we see in figure 5 that ion phase space holes are formed.

Perpendicular heating of the plasma, which is an integral part of pressure-cooker models of the downward current region, is not included in our simulation model. Instead we have increased the temperature of the ionosphere in space and the hot plate in the laboratory as a boundary condition. This yields conditions that are in agreement with observations in space. In the laboratory, this particular experiment has, so far, not been performed, but temperatures in the range used here have been measured in Q-machines. Running the simulations with different hot plate temperatures we see that the only significant difference between the results is the speed of the double layer motion, and in consequence also the time between successive double layer formations.

In space, the dominating ion species is H^+ above altitudes of a few hundred kilometres. In the experiment the ions from the discharge and Q-machine sources will be different. In order to keep the masses of the ion species as similar as possible we have chosen Ne^+ and Na^+ , which have atomic masses 20 u and 23 u respectively, for most of the simulation runs. One simulation run was performed with the Ne^+ ions replaced by He^+ . It was found that this gave rise to ion time scale waves in the part of the machine that is traversed by double layers. On the low potential side of the double layer the potential is dominated by these

waves in the experiment with the helium discharge, whereas it is dominated by a smooth ambipolar field both in space and in the experiment with a discharge in neon. To make the laboratory experiment a good representation of the space environment the ions of similar masses should be chosen.

6. Discussion

One purpose of laboratory experiments is to verify theory. In situ observations in space can only be made along the spacecraft trajectory. Even with multiple spacecraft missions like Cluster it is unlikely that the spacecraft configuration will allow simultaneous measurements at more than two points on the same auroral flux tube. Laboratory experiments offer the advantage of simultaneous access to the whole system, and the possibility of repeating the same experiment many times. By creating an experiment that is equivalent to that of the downward current region of the aurora the theories used to explain the physics of that part of space may be verified.

The laboratory experiment may also be used to study aspects of the problem that are not included in the present theoretical model. For example, there is no perpendicular heating mechanism in the model we use here. We circumvented this problem by increasing the temperature at the boundary. Hwang et al. [29] instead widened the distribution function in the μ dimension in proportion to the energy density of the parallel electric field. Both these methods produce temperatures that are consistent with observations, and they are adequate for studies of the large-scale dynamics of the system. However, neither of the methods reveals the microphysics of the heating mechanism at work. A laboratory experiment that naturally includes the relevant physics will offer the opportunity to study heating processes in the low potential plasma.

In the downward current region there is no simple current–voltage relation. A series of simulations with different voltages were shown to yield the same average current in the $V_1 < -100$ V range, where V_1 is the potential at the ionosphere, and the potential at the equatorial magnetopause is zero as usual [8]. For the upward current region there is a linear relationship found theoretically [30, 31]. Similar results have been seen in simulations, and when the voltage is close to zero the current is also small [6]. Thus we can identify two regimes of the current–voltage relationship: one with a constant current for $V_1 \lesssim -100$ V and one with a current proportional to V_1 for $V_1 \gtrsim 0$. There must be a transition region between these two regimes, and that region is not covered by our simulations. Models of the downward

current region with a constant current for V_I values below a certain negative voltage and proportional relationship above it have been used in the past [32]. Our previous simulations have verified the part of such a model where the voltage is sufficiently negative, but the behaviour in the transition region remains to be explored. It could in principle be studied using the simulation model we have used here, but only at a high computational cost. The time it takes the double layers to move through the system and form anew increases when $|V_I|$ decreases, and so does the time it takes to establish an equilibrium current. It follows that the system would have to be simulated over long periods of time to address the low voltage behaviour. We conclude that the proposed laboratory experiment is more suitable than computer simulations in the study of the current-voltage relationship for low voltages.

Satellites have observed Alfvén waves in the auroral regions [33, 34]. Numerical studies have shown that the contributions of these waves to the electron acceleration may be enough to power the aurora [35, 36]. Our simulation model is electrostatic, and it does therefore not include Alfvén waves. The proposed experiment is also limited to the study of electrostatic aspects of the aurora. It is a small, low density, device in comparison with those that are used for Alfvén wave studies [37]. Both Alfvénic and electrostatic aurora exist, and both have been observed, separately and in combination, along the same Cluster spacecraft trajectory [38]. To determine which of the two regimes is the most important in nature will require spacecraft observations. One may envision that laboratory devices that include both electrostatic and Alfvénic acceleration mechanisms may be constructed in the future, but this is beyond the scope of the experiment that is proposed here. Furthermore, it is useful to study the electrostatic effects in a dedicated experiment so that these can be distinguished from Alfvénic phenomena.

There are still questions remaining within the electrostatic framework for auroral acceleration. The picture emerging from simulations of the kind presented here is that of a dynamic return current region, where double layers are in motion all the time. In contrast, spacecraft data have sometimes been interpreted in terms of quasi-static models where the parallel electric field is supported by wave induced resistivity [9, 39]. In theory it has been shown that there is no stable equilibrium position for strong double layers with the polarity of that in the return current region [5], but what happens when the voltage is so low that double layers do not form at all is yet unknown. In our model, where the downward current region is dynamic, there are current fluctuations that increase with the applied voltage, but the mean value

of the current is voltage-independent over the voltage range investigated [8]. Quasi-static models produce a different current–voltage relationship [39]. In both cases, the current–voltage relationship is different from that of the upward current region. Even there the current–voltage relationship problem is not completely resolved. In some studies the agreement between Knight’s relation and observations has been good [40], but in others currents have been found that were several times what that theory would predict [41]. This could possibly be explained by the upward current not being in a steady state in the cases used in the latter study, indicating that the response of each of the upward and downward current regions to rapid changes in the boundary conditions remains a worthwhile research topic.

Acknowledgments

This work was supported by the Belgian Science Policy Office through the Solar–Terrestrial Centre of Excellence and by PRODEX/Cluster contract 13127/98/NL/VJ(IC)-PEA 90316. This research was conducted using the resources of the High Performance Computing Center North (HPC2N) at Umeå University in Sweden.

Appendix A. Neutral pressure

We have estimated the pressure in the main chamber of the device shown in figure 1 in order to see if it can be maintained at a level low enough to avoid collisional damping of phase space holes. We assume that the pressure in the discharge source is $p_1 = 40$ mPa [18]. The pressures in the other two sections of the device are p_2 and p_3 , and the aperture cross sections are A_1 and A_2 as shown in figure 1. We take both apertures to have the same diameter, 10 cm, each pump to have a 15 cm diameter, and we denote the pump cross section A_p . We assume two such pumps to be mounted on the main chamber and one on the small chamber between the main chamber and the source. The neutral flux through an aperture is proportional to its cross section and the pressure difference between its two sides. Equating the flux into each chamber, except the source chamber, with that out of it we arrive at this system of equations:

$$(p_2 - p_3) A_2 = 2p_3 A_p \quad (\text{A.1})$$

$$(p_1 - p_2) A_1 = (p_2 - p_3) A_2 + p_2 A_p, \quad (\text{A.2})$$

where (A.1) describes flux continuity for the main chamber and (A.2) for the chamber between the main chamber and the source. With p_1 , A_1 , A_2 , and A_p known, we solve for p_2 and p_3 and obtain

$$p_2 = \frac{p_1 A_1 (A_2 + 2A_p)}{2A_2 A_p + (A_1 + A_p) (A_2 + 2A_p)} = 9.8 \text{ mPa}, \quad (\text{A.3})$$

$$p_3 = \frac{p_1 A_1 A_2}{2A_2 A_p + (A_1 + A_p)(A_2 + 2A_p)} = 1.8 \text{ mPa. (A.4)}$$

Saeki et al. [27] examined collisional damping of an electron phase space hole by “slowly increasing the neutral pressure with helium”. In their Fig. 4, the first sign of damping appears at $p = 5.5 \times 10^{-4} \text{ torr} = 73 \text{ mPa}$. For higher pressures damping increases rapidly. Of the cases presented by Saeki, et al. [27], the highest pressure at which no damping is seen at all is $p = 2.7 \times 10^{-4} \text{ torr} = 36 \text{ mPa}$. Our estimated pressure p_1 is smaller than that by a factor of 20. For neon the collision frequency for elastic collisions between electrons and neutral neon is about double the one for helium [42], and that leaves us with a margin of a factor of 10.

Pécsele et al. [28] examined the effect of charge-exchange collisions on ion phase space holes by conducting simulations with such collisions included. Their conclusion was that “an ion vortex is damped roughly within a collision period”. The total cross section for collisions between Ne^+ ions and neutral neon is $\sigma \approx 5 \times 10^{-19} \text{ m}^{-2}$ [42]. This is the cross section at about 5 eV, which is a reasonable approximation for the ions in the ion holes. For higher energies the cross section decreases. A pressure of $p_1 = 1.8 \times 10^{-3} \text{ Pa}$ corresponds to a number density of $N = 4.3 \times 10^{17} \text{ m}^{-3}$ at a neutral temperature of 300 K, and we obtain a mean free path of $\lambda_m = 1/(N\sigma) = 4.6 \text{ m}$. The collision frequency can be estimated by $\nu = v/\lambda$, which is $\nu = 1.5 \times 10^3 \text{ s}^{-1}$ for 5 eV Ne^+ ions. The lowest plasma density in the device is $1.0 \times 10^{14} \text{ m}^{-3}$, and thus we have a lower limit of $\omega_{\text{pi}}/\nu = 2.0 \times 10^3$. Thus the ion phase space holes should be able to exist for many ion plasma periods before being damped away. For helium the cross section is lower and the ion plasma period is shorter, which would lead to a higher ω_{pi}/ν value.

Appendix B. Magnetic configuration

The magnetic field used in these simulations is the same as in [22], and it can be achieved by the coils, drawn to scale in the figure 1(b), if a current of 100 A is passed through the large diameter coils and the current for the large coils with small inner diameter on the right-hand side is 768 A. A square cross section with a side of 1 cm is assumed for the conductor. The mirror ratio is 25 with this design. The field is at its strongest at the hot plate, where $B = 0.5 \text{ T}$. Since this device has not yet been built one could imagine a different design. The purpose of the experiment is to mimic the plasma on an auroral field line, where $\dot{\mu} = 0$ holds very well. Therefore, it is important that that approximation can be made also for the experiment or else the systems would be in different regimes of physics.

The relative change of B experienced by a particle

during one gyrational period can be estimated by

$$\frac{\Delta B}{B} = v_z \frac{2\pi}{\omega_c} \frac{1}{B} \frac{dB}{dz} = \frac{2\pi m v_z}{e B^2} \frac{dB}{dz}. \quad (\text{B.1})$$

Apart from the obvious that too sharp B gradients should be avoided, we see in (B.1) that the magnitude of B , the ion mass, and to what parallel velocities the ions are accelerated are aspects that must be considered in the design.

References

- [1] Haerendel G 2011 *J. Geophys. Res. (Space Physics)* **116** A00K05
- [2] Ergun R E, Andersson L, Main D S, Su Y J, Carlsson C W, McFadden J P and Mozer F S 2002 *Physics of Plasmas* **9** 3685–3694
- [3] Andersson L, Ergun R E, Newman D L, McFadden J P, Carlsson C W and Su Y J 2002 *Physics of Plasmas* **9** 3600–3609
- [4] Raadu M A 1989 *Physics Reports* **178** 25–97
- [5] Song B, Merlino R L and D’Angelo N 1992 *Physica Scripta* **45** 391–394
- [6] Gunell H, De Keyser J, Gamby E and Mann I 2013 *Annales Geophysicae* **31** 1227–1240
- [7] Gunell H, Andersson L, Keyser J D and Mann I 2015 *Annales Geophysicae* **33** 279–293
- [8] Gunell H, Andersson L, Keyser J D and Mann I 2015 *Annales Geophysicae* **33** 1331–1342
- [9] Lynch K A, Bonnell J W, Carlson C W and Peria W J 2002 *J. Geophys. Res. (Space Physics)* **107** 1115
- [10] Hwang K J, Ergun R E, Andersson L, Newman D L and Carlson C W 2008 *J. Geophys. Res. (Space Physics)* **113** A01308
- [11] Sato N, Nakamura M and Hatakeyama R 1986 *Phys. Rev. Lett.* **57** 1227–1230
- [12] Sato N, Watanabe Y, Hatakeyama R and Mieno T 1988 *Phys. Rev. Lett.* **61** 1615–1618
- [13] Ishiguro S, Kishi Y and Sato N 1995 *Physics of Plasmas* **2** 3271–3274
- [14] Torvén S and Lindberg L 1980 *Journal of Physics D: Applied Physics* **13** 2285–2300
- [15] Torvén S and Andersson D 1979 *Journal of Physics D: Applied Physics* **12** 717–722
- [16] Torvén S 1982 *Journal of Physics D: Applied Physics* **15** 1943–1949
- [17] Schrittwieser R, Axnäs I, Carpenter T and Torvén S 1992 *IEEE Transactions on Plasma Science* **20** 607–613
- [18] Gunell H, Brenning N and Torvén S 1996 *Journal of Physics D: Applied Physics* **29** 643–654
- [19] Gunell H, Verboncoeur J P, Brenning N and Torvén S 1996 *Phys. Rev. Lett.* **77** 5059–5062
- [20] Gunell H and Löfgren T 1997 *Physics of Plasmas* **4** 2805–2812
- [21] Löfgren T and Gunell H 1998 *Physics of Plasmas* **5** 590–600
- [22] Gunell H, De Keyser J and Mann I 2013 *Physics of Plasmas* **20** 102901
- [23] Newman D L, Andersson L, Goldman M V, Ergun R E and Sen N 2008 *Physics of Plasmas* **15** 072903
- [24] Newman D L, Andersson L, Goldman M V, Ergun R E and Sen N 2008 *Physics of Plasmas* **15** 072902
- [25] Koepke M E 2002 *Physics of Plasmas* **9** 2420–2427
- [26] Rynn N, Dakin D R, Correll D L and Benford G 1974 *Phys. Rev. Lett.* **33** 765–768
- [27] Saeki K, Michelsen P, Pécsele H L and Rasmussen J J 1979 *Phys. Rev. Lett.* **42** 501–504
- [28] Pécsele H L, Trulsen J and Armstrong R J 1984 *Physica Scripta* **29** 241–253

- [29] Hwang K J, Ergun R E, Newman D L, Tao J B and Andersson L 2009 *Geophys. Res. Lett.* **36** L21104
- [30] Knight S 1973 *Planetary and Space Science* **21** 741–750
- [31] Fridman M and Lemaire J 1980 *J. Geophys. Res.* **85** 664–670
- [32] De Keyser J and Echim M 2010 *Annales Geophysicae* **28** 633–650
- [33] Keiling A, Wygant J R, Cattell C A, Mozer F S and Russell C T 2003 *Science* **299** 383–386
- [34] Chaston C C, Carlson C W, McFadden J P, Ergun R E and Strangeway R J 2007 *Geophys. Res. Lett.* **34** L07101
- [35] Watt C E J and Rankin R 2009 *Phys. Rev. Lett.* **102** 045002
- [36] Watt C E J and Rankin R 2010 *J. Geophys. Res.* **115** A07224
- [37] Gekelman W 1999 *J. Geophys. Res.* **104** 14417–14435 ISSN 2156-2202
- [38] Li B, Marklund G, Karlsson T, Sadeghi S, Lindqvist P A, Vaivads A, Fazakerley A, Zhang Y, Lucek E, Sergienko T, Nilsson H and Masson A 2013 *J. Geophys. Res. (Space Physics)* **118** 5543–5552
- [39] Jasperse J R, Basu B, Lund E J and Grossbard N 2011 *J. Geophys. Res. (Space Physics)* **116** A00K11
- [40] Frey H U, Haerendel G, Clemmons J H, Boehm M H, Vogt J, Bauer O H, Wallis D D, Blomberg L and Lühr H 1998 *J. Geophys. Res.* **103** 4303–4314
- [41] Morooka M, Mukai T and Fukunishi H 2004 *Annales Geophysicae* **22** 3641–3655
- [42] Franz G 2009 *Low pressure plasmas and microstructuring technology* (Springer Science & Business Media) ISBN: 978-3-540-85848-5